International Journal of Thermal Sciences 172 (2022) 107273

Contents lists available at ScienceDirect

International Journal of Thermal Sciences

journal homepage: www.elsevier.com/locate/ijts

Mesoscopic simulation of thermal conductivities of 3D carbon nanotubes, graphene and their epoxy resin based composites

Xueming Yang [a,*], Fanxing Meng [a], Xinyao Zhang [a], Bingyang Cao [b,**], Yao Fu [c]

[a] Hebei Key Laboratory of Low Carbon and High Efficiency Power Generation Technology, Department of Power Engineering, North China Electric Power University, Baoding, 071003, China
[b] Key Laboratory for Thermal Science and Power Engineering of Ministry of Education, Department of Engineering Mechanics, Tsinghua University, Beijing, 100084, China
[c] Department of Aerospace and Ocean Engineering, Virginia Polytechnic Institute and State University,Blacksburg, VA, 24061, USA

ARTICLE INFO

Keywords:
Thermal conductivity
Mesoscopic simulation
Carbon nanotubes
Graphene
Epoxy resin

ABSTRACT

The thermal conductivities of the 3D carbon nanotubes (CNTs), CNT/epoxy resin (CNT/EP) composites, graphene/EP composites and CNT/graphene/EP composites are systematically investigated via mesoscopic simulations using smoothed particle hydrodynamics (SPH) and dissipative particle dynamics (DPD). The effects of the CNT length and overall mass density on the thermal conductivity of the CNTs are discussed. Moreover, the influences of the loading and size of the fillers on the thermal conductivities of the CNT/EP, graphene/EP and CNTs/graphene/EP composites are investigated. The results have shown that introducing the CNT and graphene fillers simultaneously to the epoxy resin can improve the thermal conductivity of the composites most effectively. The study demonstrates that coupled DPD and SPH model is a viable approach to understand the thermal conductivities of nanocomposites at a reduced computational cost compared to full atomistic simulation.

1. Introduction

Carbon nanotubes (CNTs) and graphene have received considerable attention in the area of thermal management due to the ultrahigh thermal conductivity of individual carbon nanotube and graphene [1–3]. By adding CNTs and graphene, the thermal conductivity of the polymer composites can be improved effectively, thus CNTs and graphene are considered as promising fillers to enhance the thermal conductivity of polymer composites [4–6]. As a widely used polymer, epoxy resin (EP) has a fairly low thermal conductivity, 0.1–0.3W/(mK), which greatly limits their application in thermal management. In recent years, extensive studies have been conducted to enhance the thermal conductivities of the CNT/EP, graphene/EP and CNT/graphene/EP composites [7–10]. The thermal conductivities of these composites are closely related to the morphology parameters of CNT and/or graphene, including inherent size, density and arranged orientation. The thermal conductivities of pure CNT or graphene based macroscopic materials can be tuned by varying the morphology parameters to fabricate high thermal conductivity materials or insulation materials. Although some experimental studies [11–13] have reported the influence of morphology parameters of the CNT or graphene, they are generally hindered by certain limitations in sample preparation and testing.

Computational approaches such as molecular dynamics (MD) simulation provide an excellent route to characterize materials properties by reducing the cost of exhaustive experimentation and by providing insightful information at the molecular and microscopic scales not easily extracted from experiments. There have been many studies [13–19] on the thermal properties of pure CNT and/or graphene and related composites. However, investigating the influence of geometric and microscopic parameters on the thermal conductivity of CNT or graphene based materials, especially when CNTs networks are randomly oriented or dispersed in polymers and fluids, via MD simulations is still quite challenging due to the high computational cost.

The development of mesoscopic simulation methods, such as the dissipative particle dynamics (DPD) [20] and smoothed particle hydrodynamics (SPH) [21] provide new route to resolve this problem. Compared with MD, DPD can perform simulation over longer length and time scales through coarse-grained (CG) techniques. It can model the hydrodynamics of complex fluids and materials in the mesoscopic scale. Ionita et al. [22] investigated the dispersion homogeneity of SWCNTs in

* Corresponding author.
** Corresponding author.
E-mail addresses: xuemingyang@ncepu.edu.cn (X. Yang), caoby@tsinghua.edu.cn (B. Cao).

https://doi.org/10.1016/j.ijthermalsci.2021.107273
Received 9 October 2020; Received in revised form 10 August 2021; Accepted 6 September 2021

the EP via DPD. DPD has also been used to estimate the dispersibility of SWCNTs of various diameters within EP matrices [23,24]. Gooneie et al. [25] simulated the dispersions of carbon nanoparticles in polyamide 12 by DPD and revealed the role of aspect ratios of carbon nanoparticles in the dispersion. Zhou et al. [26] studied the dispersion and alignment of CNTs in the EP under the equilibrated and shear flow conditions using DPD. SPH is a fully Lagrangian meshless technique and has been successfully used in many research fields including astrophysics, ballistics, and micro fluidics [27–29]. Recently, Zhou et al. [30] reported the mesoscopic simulation of thermal conductivity of CNT/polymer composites by coupling SPH and DPD for the first time, where they demonstrated this hybrid method can successfully simulate the heat conduction of polymer composites.

In this work, the thermal conductivity of the CNTs bed [11], CNT/EP composites, graphene/EP composites and CNT/graphene/EP composites are investigated via mesoscopic simulations using SPH and DPD. The theoretical and experimental studies [11–13,15,18,19,31] suggested that the thermal conductivity of CNTs bed is closely related to the morphology parameters, e.g., mass density and tube length of CNTs. However, how the thermal conductivity varies with these morphology parameters is not fully understood. For example, as mentioned by Volkov et al. [16], the experimental results of the thermal conductivities reported for 3D isotropic CNT networks are out of range of the predictions by their proposed theoretical model. The DPD simulations on graphene and their based composites are also very limited, and no SPH simulations of heat conduction have been conducted in graphene-based materials to the best of our knowledge. In addition, experimental studies have reported the remarkable synergetic effect between the graphene and CNT and/or other nanomaterials fillers in improving the thermal conductivity of epoxy composites [32]. Yang et al. [33] investigated the improved thermal conductivity by adding multi-graphene platelets (MGPs) and multiwalled carbon nanotubes (MWCNTs) into epoxy composites. It is found that the MWCNT/MGP/epoxy composites exhibit a significant increase in thermal conductivity, as compared with epoxy composites with either MGPs or MWCNTs. Zhou et al. [34] also reported a better thermal conductivity enhancement performance by adding hybrid MWCNTs/micro-SiC filler into the epoxy matrix compared to adding either MWCNTs or micro-SiC.

Here we report for the first time a study on thermal conductivities of graphene/epoxy and CNT/graphene/epoxy composite via coupled DPD and SPH simulations. The effects of loading, mass density and aspect ratio of CNT or graphene on the overall thermal conductivities are discussed.

2. Methodology

In the DPD simulation, a small region of material (group of atoms) is coarse grained (CG) into a single bead, therefore the number of particles to be simulated can be greatly reduced compared with full atomistic simulations. A soft repulsion between beads i and j is described by a soft conservative force $\mathbf{F}_{ij}^{C}$. In addition, the dissipative and random forces, $\mathbf{F}_{ij}^{D}$ and $\mathbf{F}_{ij}^{R}$, effectively act as a thermostat and result in fast equilibration to the Gibbs-Boltzmann canonical ensemble. The interactions between a pair of nonbonded beads are summarized as follows:

$$f_i = \sum_{j \neq i} \left(\mathrm{F}_{ij}^{C} + \mathrm{F}_{ij}^{D} + \mathrm{F}_{ij}^{R} \right) \tag{1}$$

$$\mathrm{F}_{ij}^{C} = \begin{cases} a_{ij}(1 - r_{ij})\hat{\mathrm{r}}_{ij} & (r_{ij} < 1) \\ 0 & (r_{ij} \geq 1) \end{cases} \tag{2}$$

$$\mathrm{F}_{ij}^{D} = -\gamma w^{D}(r_{ij}) \left(\hat{r}_{ij} v_{ij} \right) \hat{r}_{ij} \tag{3}$$

$$\mathrm{F}_{ij}^{R} = \sigma w^{R}(r_{ij}) \theta_{\mathrm{ij}} \hat{r}_{ij} \tag{4}$$

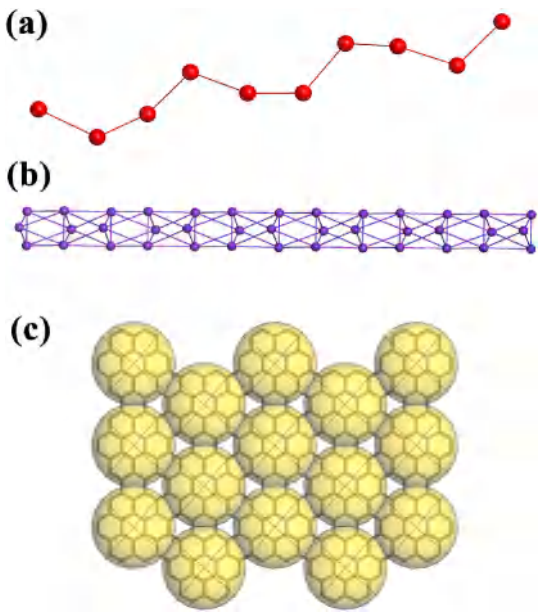

Fig. 1. Coarse-grained models: (a) a flexible epoxy resin chain; (b) SWCNT; (c) Graphene nanosheet. (For interpretation of the references to color in this figure legend, the reader is referred to the Web version of this article.)

where a_{ij} is the repulsion parameter between particles of different type; the degree of dispersion is controlled by $\Delta a = a_{ij} - a_{ii}$, where $a_{ii}$is the repulsion parameter between particles of the same type. $\mathrm{r}_{ij} = \mathrm{r}_i - \mathrm{r}_j$, $r_{ij} = |\mathrm{r}_{ij}|$, and $\hat{\mathrm{r}}_{ij} = \mathrm{r}_{ij}/r_{ij}$; $w^{D}$and $w^{R}$are weight functions dependent on r, and θ_{ij} is a white noise function; γ are the coefficients characterizing the strengths of the dissipative; $\sigma$is interpreted as the amplitude of the noise. Since$\Delta a \geq 0$, the smaller Δa means a better solubility of solutes or a better dispersion degree of the fillers in the matrix. More detailed explanation of the terms can be found in Ref. [35].

The CG model of a flexible epoxy resin chain based on bisphenol A (1 g/cm3 in mass density) is shown in Fig. 1(a). In the DPD model, ten CG beads are connected using finitely extensible nonlinear elastic (FENE) [36] springs with the bond potential of

$$\mathbf{F}_{\mathrm{ij}}^{S} = \frac{H r_{\mathrm{ij}}}{1 - \left(r_{\mathrm{ij}} / r_{\mathrm{m}} \right)^2} \tag{5}$$

where H is the spring constant, and r_{m} the maximum permissible length of one chain segment.

The CG models of SWCNT and graphene are built as shown in Fig. 1 (b) and (c), which follows the model of CNT presented by Liba et al. [37]. For both the SWCNT and graphene, 24 carbon atoms are coarsely grouped into one bead. Individual particle in the CG model of SWCNT, graphene and EP has the same volume of 480 Å^3.

In the CG model of SWCNT and graphene, Hookian spring force is used to bond neighboring beads as follows [28,35]:

$$U_{\mathrm{ij}}^{H} = K_H \left(r_{\mathrm{ij}} - r_0 \right)^2 \tag{6}$$

where K_H is the spring constant and r_0 is the equilibrium distance.

To account for the stiffness of the tube, angular potential is added in the CG model of SWCNT as follows [30,37]:

$$U_{\mathrm{i}}^{A} = K_A (\cos\theta - \cos\theta_0)^2 \tag{7}$$

where K_A is the potential constant, θ is the angle of triplets of neighboring particles, θ_0 is the equilibrium angle. The angular potential is not employed in the CG model of graphene.

Packmol software [38] is used to randomly pack the CG SWCNTs, graphene nanosheets and EP chains into the simulation box, to build the

Table 1
DPD and SPH inputs mapping from physical units.

Quantity	Dimensions	Value (DPD units)	Value (real units)
Mass	M	1	4.80×10^{-25}kg
Length	L	1	1.13×10^{-9}m
Energy	E	1	4.11×10^{-21}J
dt (DPD)	$L\sqrt{M/E}$	0.01	1.22×10^{-13}s
a_{ii} , a_{ij}	E/L	25	9.11×10^{-11}J/m
r_c	L	1	1.13×10^{-9}m
γ	$\sqrt{ME/L}$	4.5	3.33×10^{-12}kg/s
H	E/L^2	40	0.129J/m^2
r_m	L	4.0	4.52×10^{-9}m
K_H	E/L^2	2675.8	8.63J/m^2
K_A	E	38.9	1.6×10^{-19}J
r_0	L	0.6239	7.05×10^{-9}m
θ_0	–	180	180°
dt (SPH)	$L\sqrt{M/E}$	0.075	9.15×10^{-13}s
c_v	E/(MT)	1	2.87J/(kgK)

models of CNTs, CNTs/EP composites, graphene/EP composites and CNTs/graphene/EP composites.

The configurations generated from DPD simulations are employed as inputs for particle-based SPH simulations, in order to calculate the thermal conductivity. The SPH model is based on the energy part of Navier-Stokes equation given by,

$$\rho \frac{d}{dt}\left(\frac{|u|^2}{2} + e\right) = \rho f u - div(q - \tau u) \tag{8}$$

where ρ is mass density, u is the velocity, e is the internal energy per mass, f is the external force, div is divergence operator, q is local heat flux density and τ is the surface stress. In the SPH simulation of heat conduction, $u = 0$, $f = 0$, $\tau = 0$, $e = c_v T$.

Thermal conductivity in a specific direction can be computed by adding a constant amount of heat to one group of particles (hot reservoir) and subtracting heat from another (cold reservoir) under periodic boundary conditions at a regular interval. The SPH simulation performs time integration to update internal energy and local density of the particles. Temperature gradient across the simulation domain is established after sufficiently long time. Thermal conductivity is computed by Fourier law:$q = -k\nabla T$, where ∇T is the temperature gradient and k denotes the thermal conductivity.

The large-scale atomic/molecular massively parallel simulator (LAMMPS) software package [39] is used to perform the DPD and SPH simulations. The SPH-USER package in LAMMPS provides a framework and the implementation of SPH method. SPH discretises the mass distribution field into point masses, and the positions of the point masses serve as integration nodes for the field equations of continuum mechanics. To simulate the heat conduction by SPH in LAMMPS, a user command "fix sph/heat" needs to be coded and combined with the SPH-USER package for the establishment of hot and cold reservoir and to obtain the values of the added and subtracted heat. The code has been programmed by Zhou et al. [26,30] and details of the implementation

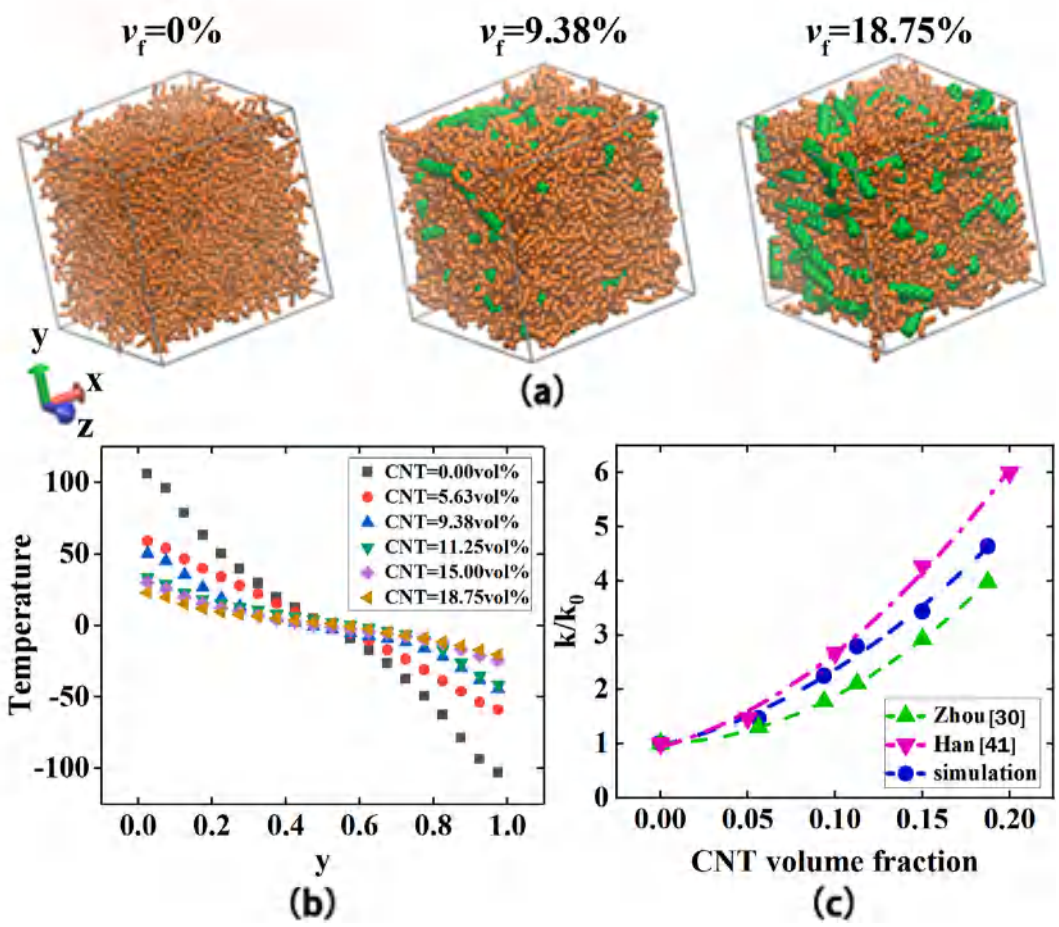

Fig. 2. (a) CG models of CNT/EP nanocomposites with different CNT volume fraction; (b) temperature profiles of CNT/EP nanocomposites; (c) relative thermal conductivities as a function of CNT volume fraction. (For interpretation of the references to color in this figure legend, the reader is referred to the Web version of this article.)

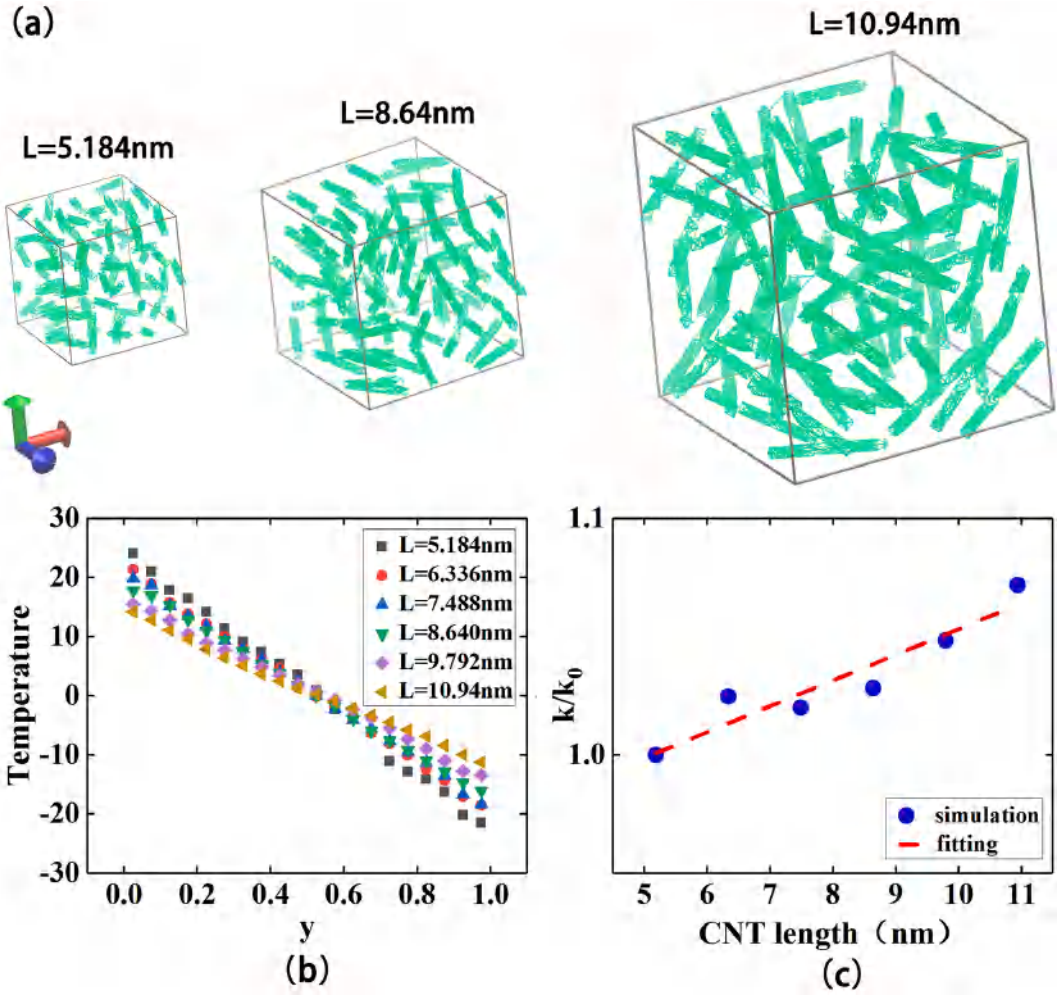

Fig. 3. (a) CG models of CNTs with different CNT length and same mass density of the system; (b) temperature profiles at different CNT length; (c) relative thermal conductivities as a function of CNT length. (For interpretation of the references to color in this figure legend, the reader is referred to the Web version of this article.)

can be found in Ref. [40]. The units and the model parameters in both the DPD and SPH simulations are listed in Table 1. The values for the listed parameters values are chosen following refs. [26,30].

3. Results and discussion

3.1. CNT/EP nanocomposites

The DPD simulations are carried out in the NVT ensemble for 1×10^5 time steps with an integration time step of 0.001 in reduced unit to achieve thermodynamic equilibrium. Then the SPH simulations are conducted to calculate the thermal conductivity of the system.

In the SPH simulations to calculate the thermal conductivity, stationary SPH particles as boundary conditions are used, and the fixed boundary conditions are applied in the heat conduction direction (y-axis) and periodic boundary conditions is adopted in the other two directions. The simulation box is subdivided into 20 slabs along the y axis. The first and the last two slabs are set as the hot side and cold side, and a constant amount of kinetic energy is added to/subtracted from the hot/cold side at a regular time interval, respectively.

A series of mesoscopic simulations is conducted to investigate the effect of the volume fraction of the CNTs on the thermal conductivity of the CNT/EP composites. First, the number of the CNTs is increased in the systems from 0 to 100 with an interval of 20, corresponding to the volume fraction of CNTs in the range of 0–18.75%. Fig. 2(a) shows the CG models of the CNT/EP composite with the volume fraction, v_f, equal to 0%, 9.38% and 18.75%, respectively. The size of the simulation box is maintained as $22 \times 22 \times 22$ in reduced unit corresponding to 24.9 nm $\times$ 24.9 nm $\times$ 24.9 nm in real size. The total particle number in the system is kept 32,000 for both pure EP and CNT/EP composites. For example, for the simulation system with a CNT volume fraction of 18.75%, the CNT/EP composite system consists of 2600 EP chains (10 particles in each chain) and 100 CNT (60 particles in each CNT).

Fig. 2(b) shows the reduced temperature profile for the pure EP and CNT/EP composite calculated via SPH simulations under the same heat flux. Since the objective of this work is to find how the thermal conductivity varies with the parameters, such as the volume fraction and length, only the relative thermal conductivity $k_r = k/k_0$ is focused on, where k is the thermal conductivity and k_0 is the first data in each thermal conductivity series investigated. The calculated k_r are shown in Fig. 2(c), in which the experimental results from Ref. [41] and the mesoscopic simulation results from Zhou et al. [30] are also provided and compared. The thermal conductivity of the composite increases with increasing volume fraction of CNTs and the calculated k_r has a quadratic relation with the volume fraction of the CNTs, i.e., $k_r \propto v_f^2$ ($k_r = 63v_f^2 + 7.6v_f + 0.96$). The calculated results are in agreement with those in Refs. [30,41], in which thermal conductivity of the CNT/EP composites has a quadratic relation with the volume fraction. The small difference between the calculated results and those by Zhou et al. [30] is likely related to the difference in the tube length, thus the computational methodology in this work is validated.

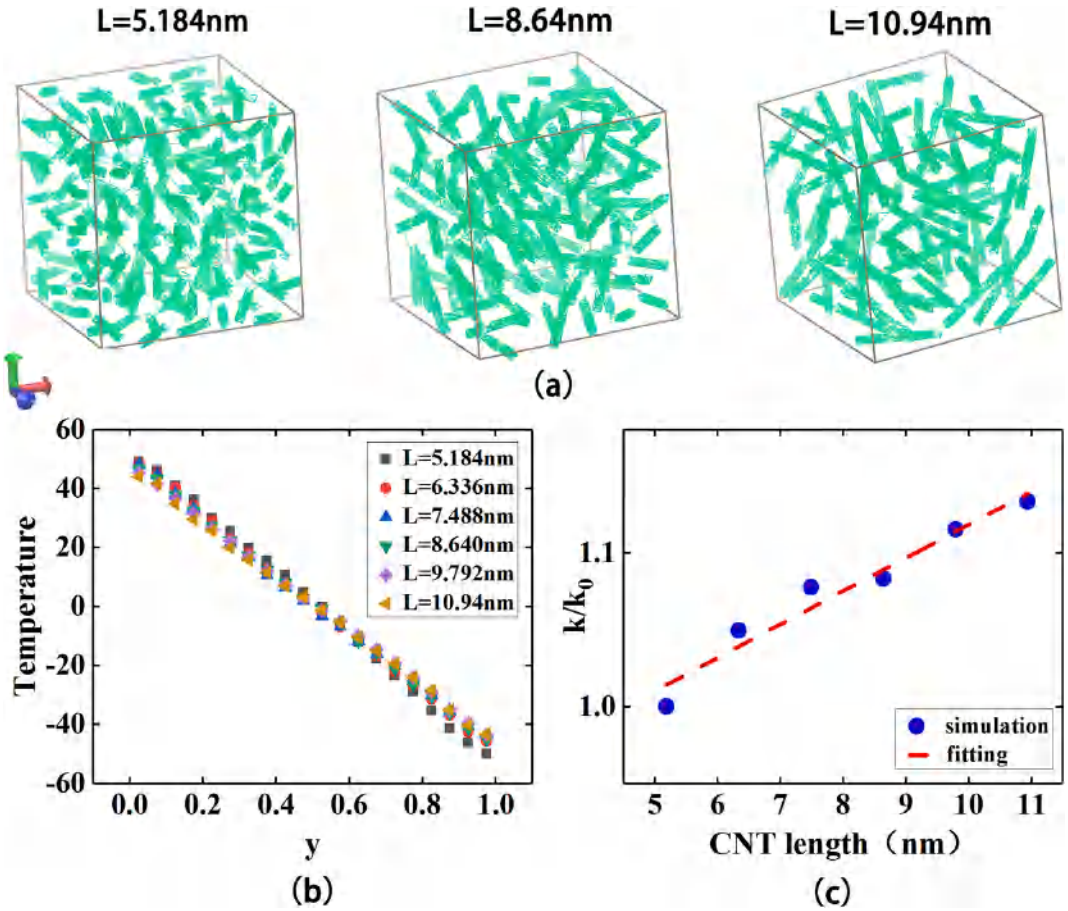

Fig. 4. (a) CG models of CNTs with different CNT length and same system size; (b) temperature profiles at different CNT length; (c) relative thermal conductivities as a function of CNT length. (For interpretation of the references to color in this figure legend, the reader is referred to the Web version of this article.)

3.2. CNTs bed

The CNTs bed is a typical randomly oriented three-dimensional (3D) network of CNTs. The CG models of CNTs bed with different CNT length and same mass density of the system are shown in Fig. 3(a). The CNTs are placed in a vacuum box, and the nanotubes can exchange heat through the interactions between the pairs of nonbonded beads.

In order to investigate the influence of the length of CNT on the thermal conductivity of CNTs, a series of mesoscopic simulation models are set up with varying CNT length from 5.184 nm to 10.94 nm while the density of the system $\rho = 0.1$ g/cm^3 and the number of CNTs $N_{CNTs} = 50$ are kept the same, as shown in Fig. 3(a). Fig. 3(b) shows the temperature profiles obtained in the heat conduction simulation. The gradient of the temperature profile decreases as the length of the CNT increases. Fig. 3 (c) shows the variation of the relative thermal conductivity of CNTs increases with their length. By fitting the data of thermal conductivity vs. CNT length, the thermal conductivity of CNTs exhibits an approximately linear relation with the CNT length.

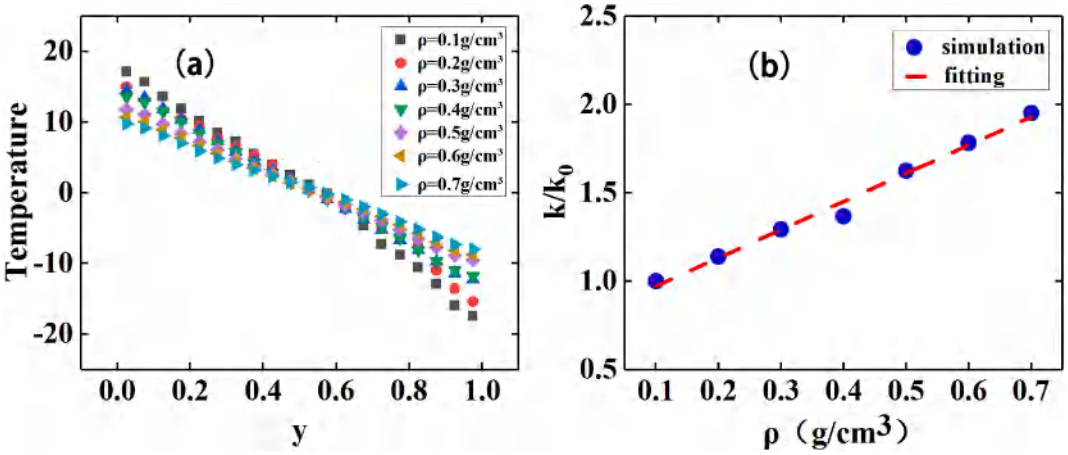

Fig. 5. (a) Temperature profiles of CNTs with different mass density; (b) relative thermal conductivities as a function of mass density. (For interpretation of the references to color in this figure legend, the reader is referred to the Web version of this article.)

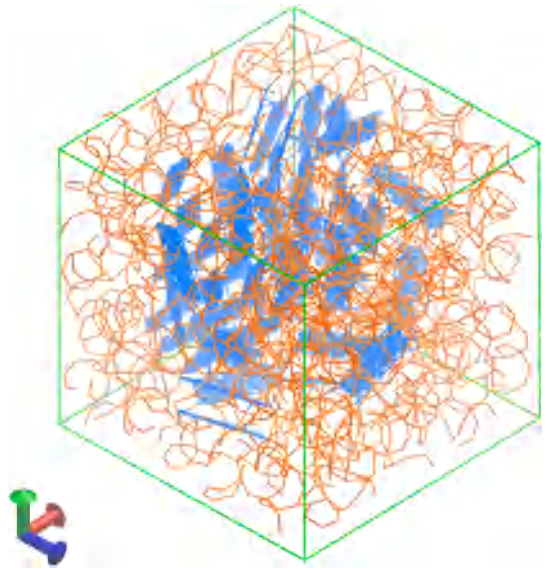

Fig. 6. Coarse-grained models of graphene/EP nanocomposites. (For interpretation of the references to color in this figure legend, the reader is referred to the Web version of this article.)

However, as shown in Fig. 3(a), the system size of the model increases with increasing CNT length to keep both the mass density and the number of the CNTs constant. In order to check whether the linear relation is caused by the system size effect, a series of mesoscopic simulations are set up with the same set of CNT length yet the system size is kept constant at a mass density $\rho = 0.1$ g/cm^3, as shown in Fig. 4 (a). It can be noticed from Fig. 4(b) the temperature profiles obtained at different tube length vary less than those in Fig. 3(b). Such a difference should be due to the different cross section area of the models. Fig. 4(c) also shows the similar linear relation between thermal conductivity and CNT length. This indicates that system size does not play significant roles in the length dependence of thermal conductivity of CNTs.

Moreover, the mass density effect on the thermal conductivity of the CNTs is investigated. Here a series of mesoscopic simulation models are set up with increasing number of the tubes from 20 to 140 with an interval of 20, thus the corresponding mass density increases from 0.1 g/cm^3 to 0.7 g/cm^3. The size of the simulation box and the tube length are kept same. The simulation results are shown in Fig. 5. It can be seen that the slope of the temperature profile becomes gradually smaller as the mass density increases. The calculated k_r shows a linear relation with the mass density, as shown in Fig. 5(b). It is worth mentioning that such a linear relation is not consistent with the nonlinear relation calculated by the theoretical model by Volkov et al. [16,17], but agrees well with our experimental results [42] of SWCNTs where $k_r \propto \rho$ was found.

3.3. Graphene/epoxy composite

A typical CG model of graphene/epoxy composite system is shown in Fig. 6. To understand the effect of the volume fraction of graphene nanosheets on the thermal conductivity of graphene/epoxy composite system, the volume fraction of fillers is changed from 0 to 18.75% by increasing the number of graphene nanosheets from 0 to 100, while keeping the total number of the particles in the system as 16,000. For

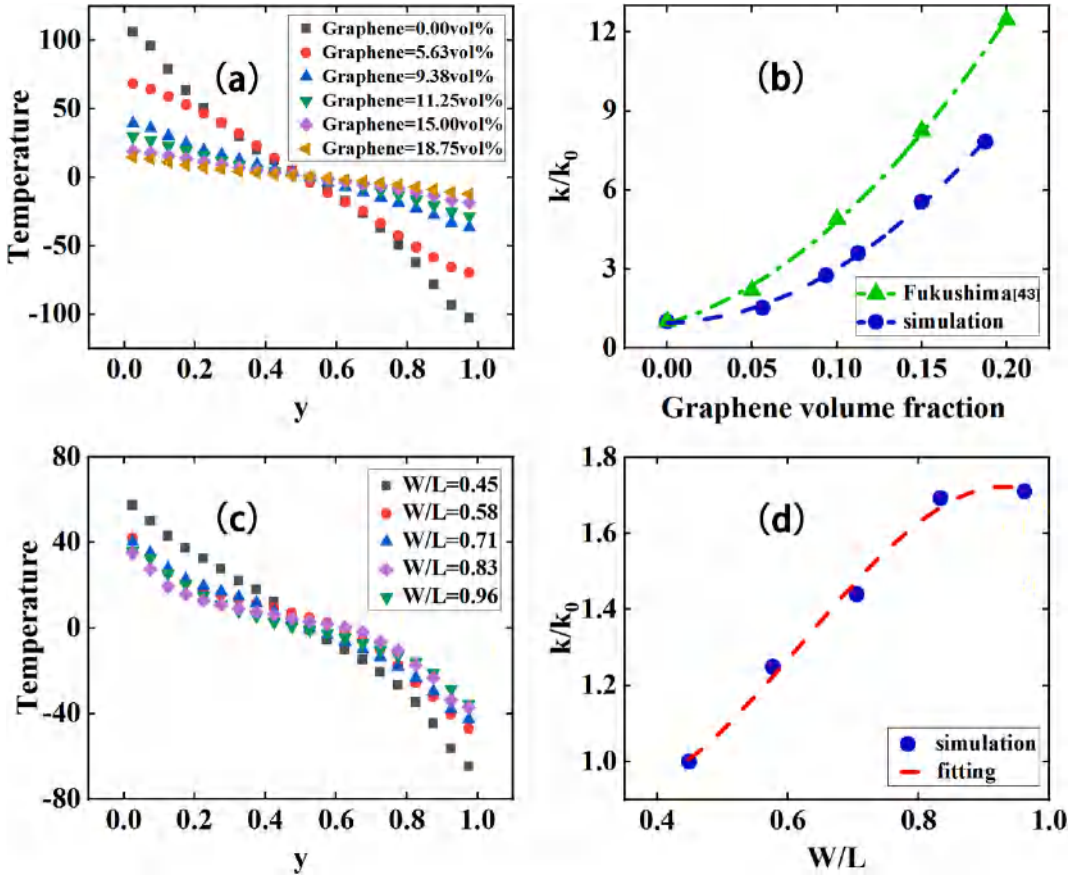

Fig. 7. (a) and (b) Temperature profiles and relative thermal conductivities of graphene/EP composites with different graphene volume fraction; (c) and (d) temperature profiles and relative thermal conductivities for graphene/EP composites with different *W/L*. (For interpretation of the references to color in this figure legend, the reader is referred to the Web version of this article.)

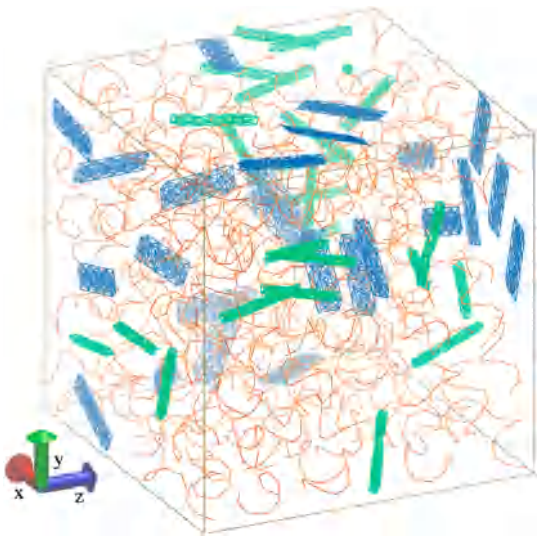

Fig. 8. Coarse-grained models of CNT/Graphene/EP nanocomposites. (For interpretation of the references to color in this figure legend, the reader is referred to the Web version of this article.)

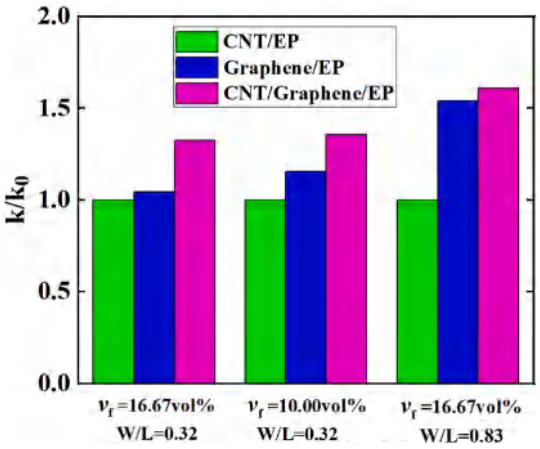

Fig. 9. Comparison of the relative thermal conductivities of CNT/graphene/EP nanocomposites with different volume fraction of CNT/Graphene and different *W/L*. (For interpretation of the references to color in this figure legend, the reader is referred to the Web version of this article.)

each graphene nanosheet, the number of the particles is 30 and the width W to length L ratio (i.e., the reciprocal of aspect ratio) of the nanosheet W/L is set as 0.32. Fig. 7 shows the relative thermal conductivity k_r versus the volume fraction of graphene nanosheets v_f. It can be seen that k_r of the graphene/epoxy composite increase with increasing v_f. A good fitting to a parabolic function indicates the thermal conductivity vs. volume fraction relation follows $k_r \propto v_f^2 (k_r = 130 v_f^2 + 7.58 v_f + 1.04)$. This is consistent with the experimental results by Fukushima et al. [43], in which thermal conductivity of the graphene/Nylon 6 composites has a quadratic relation with the volume fraction, as shown in Fig. 7(b). Our results also agree with the experimental results by Gorelov et al. [44] that the thermal conductivity of the graphene/EP composites has a quadratic relation with the mass fraction.

The thermal conductivity of single-layered graphene is closely related to the aspect ratio of graphene [45]. To examine the influence of the aspect ratio of graphene on the thermal conductivity, the width of graphene nanosheet is changed while the volume fraction and the length of graphene nanosheets are kept constant in the simulations. From Fig. 7 (b), we can see that the thermal conductivity of the composite monotonically increases with the aspect ratio W/L of graphene nanosheet. This can be explained by the lower thermal conductivity of the narrow graphene that has a stronger edge effect and boundary scattering at the edge due to its narrower width as reported by Su et al. [46]. Moreover, it also can be noticed that the increase rate of the thermal conductivity of the composite with the aspect ratio W/L will be slower when the shape of graphene is close to the square shape.

3.4. CNT/graphene/epoxy composite

Here the mesoscopic simulation based on DPD and SPH are conducted to compare the thermal conductivity of the CNT/epoxy, graphene/epoxy and CNT/graphene/epoxy nanocomposite. A typical CG model of CNT/graphene/epoxy system is shown in Fig. 8. In the simulations, the total number of the DPD particles in the systems is kept the same as 7200. The lengths of the tubes and the graphene nanosheets are 5.184 nm. Three models are set up for comparison: (1) $v_f = 16.67\%$, $W/L = 0.32$; (2) $v_f = 10\%$, $W/L = 0.32$; (3) $v_f = 16.67\%$, $W/L = 0.83$. Here the volume fraction of the fillers in CNT/graphene/epoxy composite is the same. Fig. 9 shows the comparison of the simulation results. It can be observed that the thermal conductivity of the graphene nanosheet is higher than that of the CNT at the same $v_f$while the CNT/graphene/epoxy nanocomposite exhibits the largest thermal conductivity. This indicates that synergetic effect between the graphene and CNT can improve the thermal conductivity of the composites, which is consistent with the conclusions in experimental studies [33].

4. Conclusions

In this study, the thermal conductivities of CNTs, graphene/EP and CNT/graphene/epoxy composites are investigated by mesoscopic simulations using DPD and SPH for the first time. An analysis of how the size and volume fraction of fillers affect the thermal conductivity of CNTs and/or graphene-based epoxy resin composites are presented. Such investigations can facilitate the understanding of the mechanism and microscopic parameters that govern the thermal conductivity of CNT and/or graphene-based materials at a larger scale. The proposed CG model holds the advantage of significantly reducing computational cost compared to full atomistic simulation. For example, the system of pure EP (as shown in Fig. 2(a)) contains a total atom number of 1,280,000. A full atomistic MD simulation of such a system is thus very computationally demanding. In fact, even a typical full atomistic MD simulation of heat conduction for a pure EP system containing about 4000 atoms requires 18 h with 12 cores; for an EP system with 1,280,000 atoms, it would require thousands of hours with the same of number of cores. However, the DPD and SPH simulations for such a large system only need 900s (0.25h) using 12 cores, which is approximately 0.04% of that needed for full atomistic model.

Moreover, this work demonstrates that the mesoscopic simulation using DPD and SPH, which bridges the atomistic and continuum simulation, can be an effective tool in analyzing the thermal conductivity of nanocomposites. However, it should be acknowledged that mesoscopic simulations using DPD and SPH for heat conduction analysis is still under rapid development and less mature compared to MD methods, therefore it deserves further study in order to be extensively applied in understanding heat transport phenomena.

Declaration of competing interest

The authors declare that they have no known competing financial interests or personal relationships that could have appeared to influence the work reported in this paper.

Data availability

Data will be made available on request.

Acknowledgments

The author Dr. Yang gratefully acknowledges the support from the National Natural Science Foundation of China (Grant Nos. 52076080 and 51576066) and the Natural Science Foundation of Hebei Province of China (Grant No. E2019502138).

References

[1] X. Pan, L. Shen, A.P.H.J. Schenning, C.W.M. Bastiaansen, Transparent, high-thermal-conductivity ultradrawn polyethylene/graphene nanocomposite films, Adv. Mater. 31 (2019) 1904348.
[2] Y. Li, J. Chen, X. Xie, Y. Xing, J. Song, Thermal management for purification of aligned arrays of single-walled carbon nanotubes based on thermocapillary flow by pulsed heating, Int. J. Therm. Sci. 138 (2019) 480–486.
[3] A. Hussain, I.H. Abidi, C.Y. Tso, K.C. Chan, Z. Luo, C.Y.H. Chao, Thermal management of lithium ion batteries using graphene coated nickel foam saturated with phase change materials, Int. J. Therm. Sci. 124 (2018) 23–35.
[4] S. Ramakrishnan, X. Wang, J. Sanjayan, Effects of various carbon additives on the thermal storage performance of form-stable PCM integrated cementitious composites, Appl. Therm. Eng. 148 (2019) 491–501.
[5] T. Luo, J.R. Lloyd, Enhancement of thermal energy transport across graphene/graphite and polymer interfaces: a molecular dynamics study, Adv. Funct. Mater. 22 (2012) 2495–2502.
[6] Y. Zhang, Y. Ren, H. Guo, S. Bai, Enhanced thermal properties of PDMS composites containing vertically aligned graphene tubes, Appl. Therm. Eng. 150 (2019) 840–848.
[7] X. Shen, Z. Wang, Y. Wu, X. Liu, Y. He, J. Kim, Multilayer graphene enables higher efficiency in improving thermal conductivities of graphene/epoxy composites, Nano Lett. 16 (2016) 3585–3593.
[8] S. Mohammad Nejad, R. Srivastava, F.M. Bellussi, H. Chávez Thielemann, P. Asinari, M. Fasano, Nanoscale thermal properties of carbon nanotubes/epoxy composites by atomistic simulations, Int. J. Therm. Sci. 159 (2021) 106588.
[9] H. Hou, W. Dai, Q. Yan, L. Lv, F.E. Alam, M. Yang, Y. Yao, X. Zeng, J. Xu, J. Yu, N. Jiang, C. Lin, Graphene size-dependent modulation of graphene frameworks contributing to the superior thermal conductivity of epoxy composites, J. Mater. Chem. 6 (2018) 12091–12097.
[10] X. Yang, X. Wang, W. Wang, Y. Fu, Q. Xie, Atomic-scale insights into interface thermal resistance between epoxy and boron nitride in nanocomposites, Int. J. Heat Mass Tran. 159 (2020) 120105.
[11] R.S. Prasher, X.J. Hu, Y. Chalopin, N. Mingo, K. Lofgreen, S. Volz, F. Cleri, P. Keblinski, Turning carbon nanotubes from exceptional heat conductors into insulators, Phys. Rev. Lett. 102 (2009) 105901.
[12] A.N. Omrani, E. Esmaeilzadeh, M. Jafari, A. Behzadmehr, Effects of multi walled carbon nanotubes shape and size on thermal conductivity and viscosity of nanofluids, Diam. Relat. Mater. 93 (2019) 96–104.
[13] S. Ligati, A. Ohayon-Lavi, J. Keyes, G. Ziskind, O. Regev, Enhancing thermal conductivity in graphene-loaded paint: effects of phase change, rheology and filler size, Int. J. Therm. Sci. 153 (2020) 106381.
[14] X. Yang, D. Chen, Z. Han, X. Ma, A.C. To, Effects of welding on thermal conductivity of randomly oriented carbon nanotube networks, Int. J. Heat Mass Tran. 70 (2014) 803–810.
[15] Y. Chalopin, S. Volz, N. Mingo, Erratum: "Upper bound to the thermal conductivity of carbon nanotube pellets, 084301, J. Appl. Phys. 105 (2009) 39902.)], J. Appl. Phys. 108 (2010.
[16] A.N. Volkov, L.V. Zhigilei, Scaling laws and mesoscopic modeling of thermal conductivity in carbon nanotube materials, Phys. Rev. Lett. 104 (2010) 215902.
[17] O.R.T.U. A.N. Volkov, L.V. Zhigilei, Oak Ridge National Lab. ORNL, Heat conduction in carbon nanotube materials: strong effect of intrinsic thermal conductivity of carbon nanotubes Appl. Phys. Lett. 101 (2012) 43113.
[18] X.M. Yang, X.Y. Zhang, B.Y. Cao, The effect of thermal contact number on the tube-tube contact conductance of single-walled carbon nanotubes, Nanomaterials 9 (3) (2019) 477.
[19] H.L. Zhong, J.R. Lukes, Interfacial thermal resistance between carbon nanotubes: molecular dynamics simulations and analytical thermal modeling, Phys. Rev. B 74 (2006) 125403–125410.
[20] P. Español, P. Warren, Statistical mechanics of dissipative particle dynamics, Europhys. Lett. 30 (1995) 191–196.
[21] J.J. Monaghan, Smoothed particle hydrodynamics, Annu. Rev. Astron. Astrophys. 30 (1992) 543–574.
[22] M. Ionita, Multiscale molecular modeling of SWCNTs/epoxy resin composites mechanical behaviour, Compos. B Eng. 43 (2012) 3491–3496.
[23] A. Maiti, J. Wescott, P. Kung, Nanotube–polymer composites: insights from Flory–Huggins theory and mesoscale simulations, Mol. Simulat. 31 (2005) 143–149.
[24] K. Lee, H.J. Lim, S.J. Yang, Y.S. Kim, C.R. Park, Determination of solubility parameters of single-walled and double-walled carbon nanotubes using a finite-length model, RSC Adv. 3 (2013) 4814.
[25] A. Gooneie, R. Hufenus, Hybrid carbon nanoparticles in polymer matrix for efficient connected networks: self-assembly and continuous pathways, Macromolecules 51 (2018) 3547–3562.
[26] B. Zhou, W. Luo, J. Yang, X. Duan, Y. Wen, H. Zhou, R. Chen, B. Shan, Simulation of dispersion and alignment of carbon nanotubes in polymer flow using dissipative particle dynamics, Comput. Mater. Sci. 126 (2017) 35–42.
[27] M.B. Liu, G.R. Liu, Z. Zong, K.Y. Lam, Computer simulation of high explosive explosion using smoothed particle hydrodynamics methodology, Comput. Fluids 32 (2003) 305–322.
[28] C.E. Zhou, G.R. Liu, K.Y. Lou, Three-dimensional penetration simulation using smoothed particle hydrodynamics, Int. J. Comp. Meth.-Sing. 4 (2011) 671–691.
[29] M.B. Liu, G.R. Liu, Meshfree particle simulation of micro channel flows with surface tension, Comput. Mech. 35 (2005) 332–341.
[30] B. Zhou, W. Luo, J. Yang, X. Duan, Y. Wen, H. Zhou, R. Chen, B. Shan, Thermal conductivity of aligned CNT/polymer composites using mesoscopic simulation, Compos. Part A Appl. Sci. Manuf. 90 (2016) 410–416.
[31] Y. Chalopin, S. Volz, N. Mingo, Upper bound to the thermal conductivity of carbon nanotube pellets, J. Appl. Phys. 105 (2009) 84301.
[32] G. Lee, M. Park, J. Kim, J.I. Lee, H.G. Yoon, Enhanced thermal conductivity of polymer composites filled with hybrid filler, Compos. Part A Appl. Sci. Manuf. 37 (2006) 727–734.
[33] S. Yang, W. Lin, Y. Huang, H. Tien, J. Wang, C.M. Ma, S. Li, Y. Wang, Synergetic effects of graphene platelets and carbon nanotubes on the mechanical and thermal properties of epoxy composites, Carbon 49 (2011) 793–803.
[34] T. Zhou, X. Wang, X. Liu, D. Xiong, Improved thermal conductivity of epoxy composites using a hybrid multi-walled carbon nanotube/micro-SiC filler, Carbon 48 (2010) 1171–1176.
[35] R.D. Groot, P.B. Warren, Dissipative particle dynamics: bridging the gap between atomistic and mesoscopic simulation, J. Chem. Phys. 107 (1997) 4423–4435.
[36] J. Qiu, C. Zhang, B. Wang, R. Liang, Investigation of the flow behaviors of carbon nanotubes dispersed epoxy resin with modified bi-mode FENE dumbbell simulation, Comput. Mater. Sci. 44 (2009) 1379–1385.
[37] O. Liba, D. Kauzlarić, Z.R. Abrams, Y. Hanein, A. Greiner, J.G. Korvink, A dissipative particle dynamics model of carbon nanotubes, Mol. Simulat. 34 (2008) 737–748.
[38] L. Martinez, R. Andrade, E.G. Birgin, J.M. Martinez, PACKMOL: a package for building initial configurations for molecular dynamics simulations, J. Comput. Chem. 30 (2009) 2157–2164.
[39] S. Plimpton, Fast parallel algorithms for short-range molecular dynamics, J. Comput. Phys. 117 (1995) 1–19.
[40] B. Zhou, Simulation of rheological properties of polymers via dissipative particle dynamics. Diss. Master Thesis, Huazhong University of Science & Technology, 2016.
[41] Z.D. Han, A. Fina, Thermal conductivity of carbon nanotubes and their polymer nanocomposites: a review, Prog. Polym. Sci. 36 (7) (2011) 914–944.
[42] X. Yang, J. Cui, K. Xue, Y. Fu, H. Li, H. Yang, Thermal conductivity and thermoelectric properties in 3D macroscopic pure carbon nanotube materials, Nanotechnol. Rev. 10 (1) (2021) 178–186.
[43] H. Fukushima, L.T. Drzal, B.P. Rook, M.J. Rich, Thermal conductivity of exfoliated graphite nanocomposites, J. Therm. Anal. Calorim. 85 (2006) 235–238.
[44] B. Gorelov, A. Gorb, A. Nadtochiy, D. Starokadomsky, V. Kuryliuk, N. Sigareva, O. Polovina, Epoxy filled with bare and oxidized multi-layered graphene nanoplatelets: a comparative study of filler loading impact on thermal properties, J. Mater. Sci. 54 (12) (2019) 9247–9266.
[45] D.L. Nika, A.S. Askerov, A.A. Balandin, Anomalous size dependence of the thermal conductivity of graphene ribbons, Nano Lett. 12 (2012) 3238–3244.
[46] R. Su, X. Zhang, Size effect of thermal conductivity in monolayer graphene, Appl. Therm. Eng. 144 (2018) 488–494.